First Determination of the 8Li Valence Neutron Asymptotic Normalization Coefficient Using the 7Li(8Li,7Li)8Li Reaction

D. Howell, B. Davids, J. P. Greene, R. Kanungo, S. Mythili, C. Ruiz, G. Ruprecht, I. J. Thompson

February 27, 2013

Disclaimer

This document was prepared as an account of work sponsored by an agency of the United States government. Neither the United States government nor Lawrence Livermore National Security, LLC, nor any of their employees makes any warranty, expressed or implied, or assumes any legal liability or responsibility for the accuracy, completeness, or usefulness of any information, apparatus, product, or process disclosed, or represents that its use would not infringe privately owned rights. Reference herein to any specific commercial product, process, or service by trade name, trademark, manufacturer, or otherwise does not necessarily constitute or imply its endorsement, recommendation, or favoring by the United States government or Lawrence Livermore National Security, LLC. The views and opinions of authors expressed herein do not necessarily state or reflect those of the United States government or Lawrence Livermore National Security, LLC, and shall not be used for advertising or product endorsement purposes.

First Determination of the ^{8}Li Valence Neutron Asymptotic Normalization Coefficient Using the ^{7}Li(^{8}Li,^{7}Li)^{8}Li Reaction.

D. Howell,[1,2] B. Davids,[2] J. P. Greene,[3] R. Kanungo,[4] S. Mythili,[2] C. Ruiz,[2] G. Ruprecht,[2] and I. J. Thompson[5]

[1]*Department of Physics, Simon Fraser University,*

Burnaby, British Columbia, Canada

[2]*TRIUMF, Vancouver, British Columbia, Canada*

[3]*Physics Division, Argonne National Laboratory, Argonne, Illinois 60439, USA*

[4]*Astronomy and Physics Department, Saint Mary's University,*

Halifax, Nova Scotia B3H 3C3, Canada

[5]*Lawrence Livermore National Laboratory L-414, Livermore, California 94551, USA*

(Dated: February 21, 2013)

Abstract

We report here a determination of the asymptotic normalization coefficient of the valence neutron in ^{8}Li from a measurement of the angular distribution of the ^{7}Li(^{8}Li,^{7}Li)^{8}Li reaction at 11 MeV. Using isospin symmetry the ^{8}B ANC has also been calculated and used to infer a value for $S_{17}(0)$ of 20.2 ± 4.4 eV b.

PACS numbers: 25.70.Hi, 26.20.+f, 26.65.+t, 27.20.+n

The rates of many solar fusion reactions are still quite uncertain. Excluding the hep reaction, the decay of ^{8}B produces the highest energy solar neutrinos measured by SNO and Super-K [1]. ^{8}B is produced via the ^{7}Be(p,γ)^{8}B reaction from the ppIII branch of the pp chains. Therefore, predicted experimental neutrino rates from the β^+ decay of ^{8}B are proportional to the rate of the ^{7}Be(p,γ)^{8}B radiative capture reaction, which at astrophysically relevant energies is the most poorly known of all reactions of the pp chains. This single reaction rate uncertainty introduces a 7.5% uncertainty into the calculations for the theoretical rates for Super-K and SNO [1]. The purpose of this study is to make an indirect measurement of $S_{17}(0)$, the zero energy astrophysical S-factor describing the ^{7}Be(p,γ)^{8}B reaction, from the elastic transfer reaction ^{7}Li(^{8}Li,^{7}Li)^{8}Li.

$S_{17}(0)$ has previously been derived from measurements of radiative capture, Coulomb breakup, and transfer reactions. Radiative capture measurements have been performed at relative kinetic energies as low as 117 keV [2] to obtain values for $S_{17}(0)$, but have been limited by large uncertainties both experimentally and theoretically when extrapolating down to relevant solar energies. Indirect measurements of theoretically related reactions provide other methods of inferring the S-factor and while subject to different systematic uncertainties, do not require extrapolation.

The interference between elastic scattering and neutron transfer in the ^{7}Li(^{8}Li,^{7}Li)^{8}Li reaction produces characteristic oscillations in the differential cross section as a function of the scattering angle. From the analysis of the differential cross section the asymptotic normalization coefficient (ANC) for the valence neutron in ^{8}Li can be determined and used to derive the ^{8}B valence proton ANC, which may be used to infer a value for $S_{17}(0)$.

I. THEORY

A brief primer based on Reference [3] of the theory used to extract ANCs within a distorted wave Born approximation (DWBA) framework is presented here. We consider the reaction

$$X + A \rightarrow Y + B, \tag{1}$$

where $X = Y + a$, $B = A + a$, and a is the transferred particle. The entrance channel ANC, $C^X_{Yal_Xj_X}$, may be calculated from the single particle ANC, $b_{Yal_Xj_X}$, and the spectroscopic

factor, $S_{Yal_Xj_X}$.

$$\left(C^X_{Yal_Xj_X}\right)^2 = S_{Yal_Xj_X}b^2_{Yal_Xj_X}, \tag{2}$$

where j_X is the total angular momentum of particle a in the nucleus X, and l_X is the orbital angular momentum of the relative motion of particles Y and a in the bound state $X = (Ya)$.

By writing the ANC in this form the calculated DWBA differential cross section's dependence on the geometry of the bound state wavefunction is significantly reduced [3]. To illustrate this, the differential cross section can be written as

$$\frac{d\sigma}{d\Omega} = \sum_{j_Bj_X} \frac{(C^B_{Aal_Bj_B})^2}{b^2_{Aal_Bj_B}} \frac{(C^X_{Yal_Xj_X})^2}{b^2_{Yal_Xj_X}}\sigma^{DW}_{l_Bj_Bl_Xj_X}. \tag{3}$$

For peripheral reactions, only values where $r_{Ya} > R_X$ and $r_{Aa} > R_B$ will contribute to the DWBA radial integrals, where r_{Ya} and r_{Aa} are the separations, and R_X and R_B represent the nuclear interaction radii between the constituents of both nuclei X and B. Therefore, each of the bound state wavefunctions entering the expression for the DWBA cross section $\sigma^{DW}_{l_Bj_Bl_Xj_X}$ can be approximated by its asymptotic form, with the product of the single particle ANCs containing the only dependence on the geometry of the bound state potentials. Reparameterizing the differential cross section as

$$\frac{d\sigma}{d\Omega} = \sum_{j_Bj_X}(C^B_{Aal_Bj_B})^2(C^X_{Yal_Xj_X})^2 R_{l_Bj_Bl_Xj_X}, \tag{4}$$

the factor

$$R_{l_Bj_Bl_Xj_X} = \frac{\sigma^{DW}_{l_Bj_Bl_Xj_X}}{b^2_{Aal_Bj_B}b^2_{Yal_Xj_X}} \tag{5}$$

contains all the dependence on the geometry of the bound state potentials. This results in the parameterization of the peripheral reaction differential cross section in terms of the ANCs of the initial and final states which are insensitive to the geometries of the bound state potentials [3].

For the specific case of the ^{7}Be$(p,\gamma)^8$B reaction, the numerical relationship between $S_{17}(0)$ and the ^{8}B ANCs can be expressed by the relationship [4, 5],

$$S_{17}(0) = 38.6(C^2_{p_{1/2}}(^8B) + C^2_{p_{3/2}}(^8B))\,\text{eV b fm}, \tag{6}$$

where $C_{p_{1/2}}(^8B) \equiv C^{^8B}_{^7Be\,p\,1\frac{1}{2}}$ and $C_{p_{3/2}}(^8B) \equiv C^{^8B}_{^7Be\,p\,1\frac{3}{2}}$.

II. EXPERIMENT

The benefit of studying the $^7\text{Li}(^8\text{Li},^7\text{Li})^8\text{Li}$ reaction is apparent upon examination of Equation 3. The two ANC terms $C^B_{Aal_Bj_B}$ and $C^X_{Yal_Xj_X}$, as well as the single particle ANC terms $b_{Aal_Bj_B}$ and $b_{Yal_Xj_X}$, are identical for this reaction thereby simplifying the expression and reducing the associated uncertainties.

The experiment was performed using the TUDA (TRIUMF-U.K. Detector Array) chamber in the ISAC I facility at TRIUMF in Vancouver, BC, Canada. A $^8\text{Li}^{2+}$ beam at an energy of 11 MeV with a beam current ranging from 3 - 5 pA was used. Two annular detectors were used; a LEDA detector and a S2 detector. The TUDA chamber was specifically designed for use with the Louvain-Edinburgh Detector Array [6] (LEDA), which consists of 8 separate sectors each with 16 elements. The S2 is a double sided silicon strip detector consisting of a single element that is divided into 16 sectors on the backside and 48 rings on the front.

As shown in Figure 1, within the TUDA chamber the LEDA and S2 detectors were mounted downstream from the target ladder at 72 mm and 130 mm respectively, resulting in an angular coverage of 36 - 60 degrees for the LEDA and 5 - 15 degrees for the S2, both in the laboratory frame. The target used was $25\,\mu\text{g/cm}^2$ ^7LiF on a $10\,\mu\text{g/cm}^2$ carbon backing.
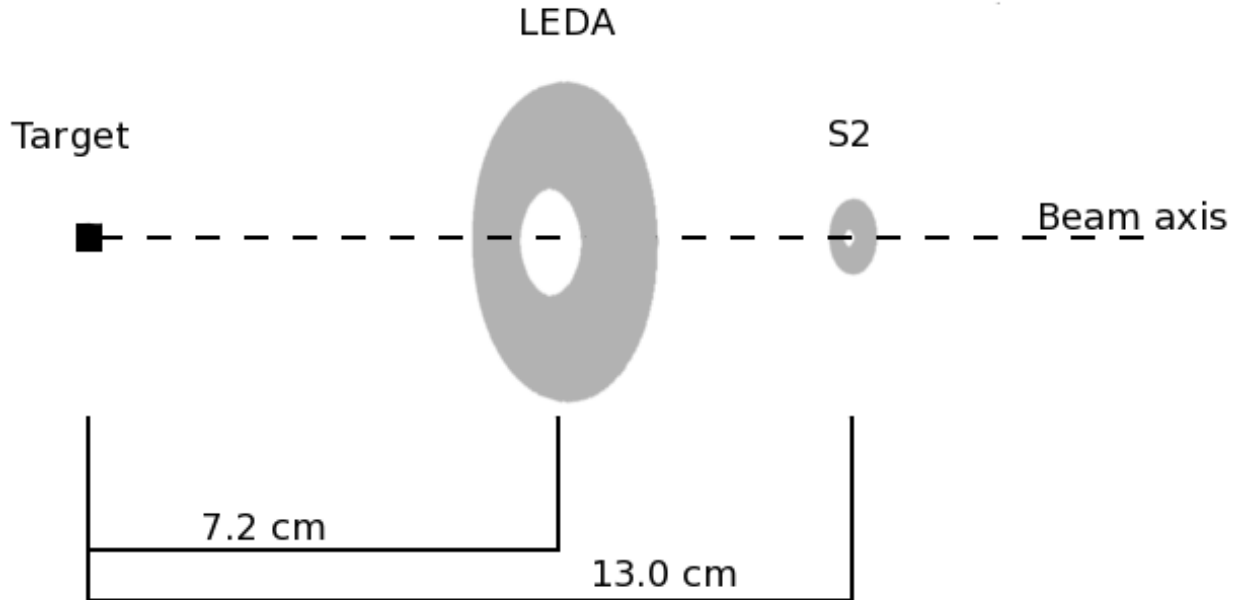

FIG. 1: Experimental setup of the LEDA and S2 detectors in the TUDA chamber.

The presence of ^{19}F in the target gave rise to elastic scattering which was analyzed for calibration of both detectors. Comparing the absolute number of ^{8}Li elastically scattered from ^{19}F detected in the S2 detector between laboratory angles of 5 to 15 degrees an asymmetry was observed among the different sectors. This asymmetry is the result of a slight shift in the beam spot from the center of the detectors.

Using the data from ^{8}Li elastically scattered from ^{19}F, an analysis was performed to determine the displacement of each detector with respect to the beam axis. By varying the offset values and thus the correlated scattering angle the asymmetry was minimized and the beam offset was determined. The offset was found to be 0.05 ± 0.02 cm in the horizontal and 0.13 ± 0.01 cm in the vertical for the S2 detector. Due to the smaller statistics and reduced angular resolution in the LEDA its beam offset was difficult to determine precisely. Values obtained for the offset in the LEDA were 0.05 ± 0.05 cm in the horizontal and 0.10 ± 0.05 cm in the vertical. When comparing the offset LEDA data to the zero offset case no significant difference was observed. Therefore, in order to reduce the introduction of systematic errors associated with correcting for the offset in the LEDA the offset was neglected.

III.   ANALYSIS

Reduction of the S2 data was performed via energy and time gates. An energy gate was placed on ring and sector energies ensuring agreement between the two channels within 3%. Further background reduction was achieved through timing cuts. Identification of various peaks in the TDC spectra was done by placing tight windows on known loci in the energy spectrum and assessing the corresponding peaks in the timing data. The data collected in the S2 following background reduction are shown in Figure 2.

Even though the S2 detector subtended scattering angles between 5 and 15 degrees in the laboratory frame, the kinematics of the reactions made separating the elastic lithium locus from the stronger carbon and fluorine elastic loci impossible at angles below 9 degrees. From 9 degrees and up the lithium peak is sufficiently separated from the other peaks to perform a reliable multiple peak fit.

The components in the S2 fit include: a gaussian for ^{8}Li and ^{7}Li from the ^{8}Li + ^{7}Li reaction, gaussians for ^{8}Li elastic scattering from ^{12}C and ^{19}F, as well as linear and gaussian backgrounds. The background gaussian describes a small peak with a nearly uniform energy
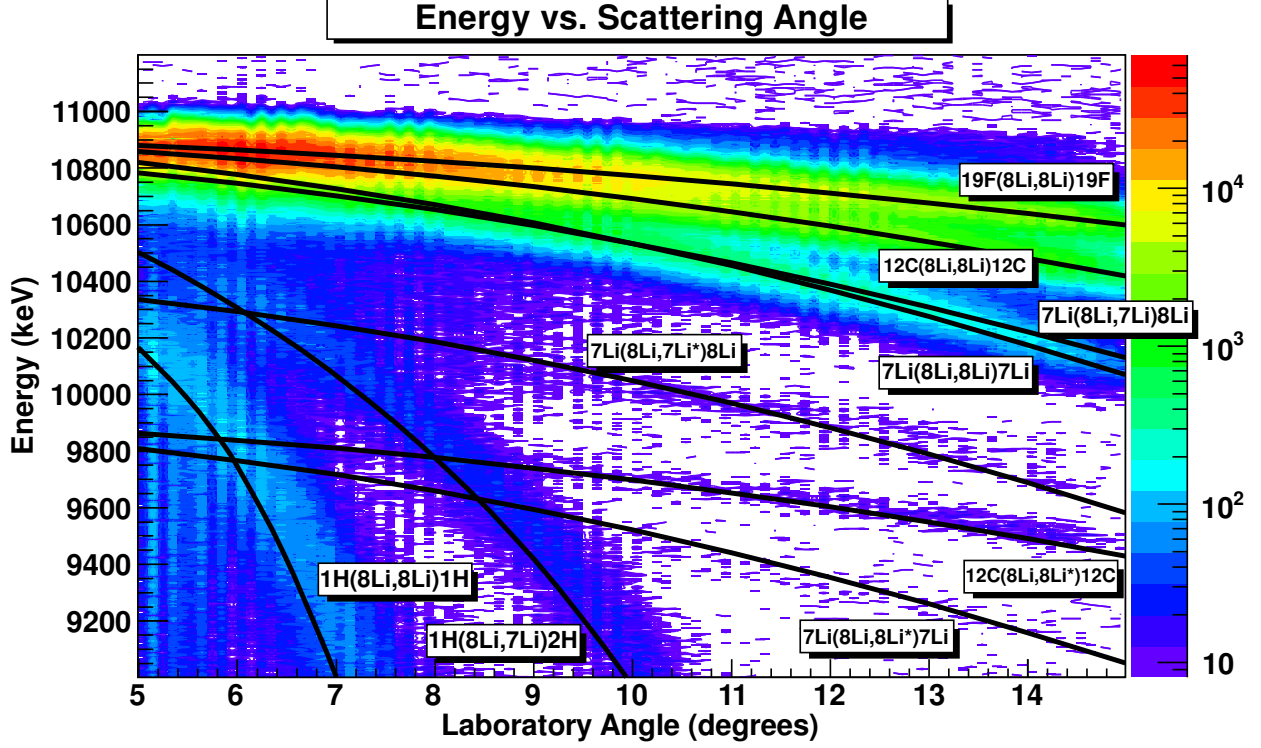
FIG. 2: Identified loci in the S2 detector following background reduction.

profile over the entire angular range which we attribute to elastic scattering from heavy contaminants; Fe, Te, Ba, and Pb were all known to be present in the target at trace levels. A typical multiple peak fit for the S2 data is shown in Figure 3. The small excess of events above the fit at the low energy tail of the "Li Exchange" peak amounts to only 0.37% of the total ^{8}Li and ^{7}Li events from the ^{7}Li(^{8}Li,^{7}Li)^{8}Li reaction deduced from the fit.

^{8}Li was detected with the LEDA detector in coincidence with ^{7}Li in the same detector, allowing us to easily separate these events from the background. Following the detection of an event consistent with ^{8}Li and a coincidence consistent with ^{7}Li, the individual energies were summed and compared to the expected total energy. The total energy gate was corrected for energy loss through the target and dead layer of the LEDA detector based on SRIM energy loss calculations [7].

Figure 4 shows the detected coincidences of ^{8}Li and ^{7}Li in the LEDA detector. The top figure depicts the full range of detected coincidences, while the lower figures display projections at 41.0 and 50.5 degrees. Due to the coincidence requirement and the total energy gate the background in the LEDA was effectively reduced to zero.
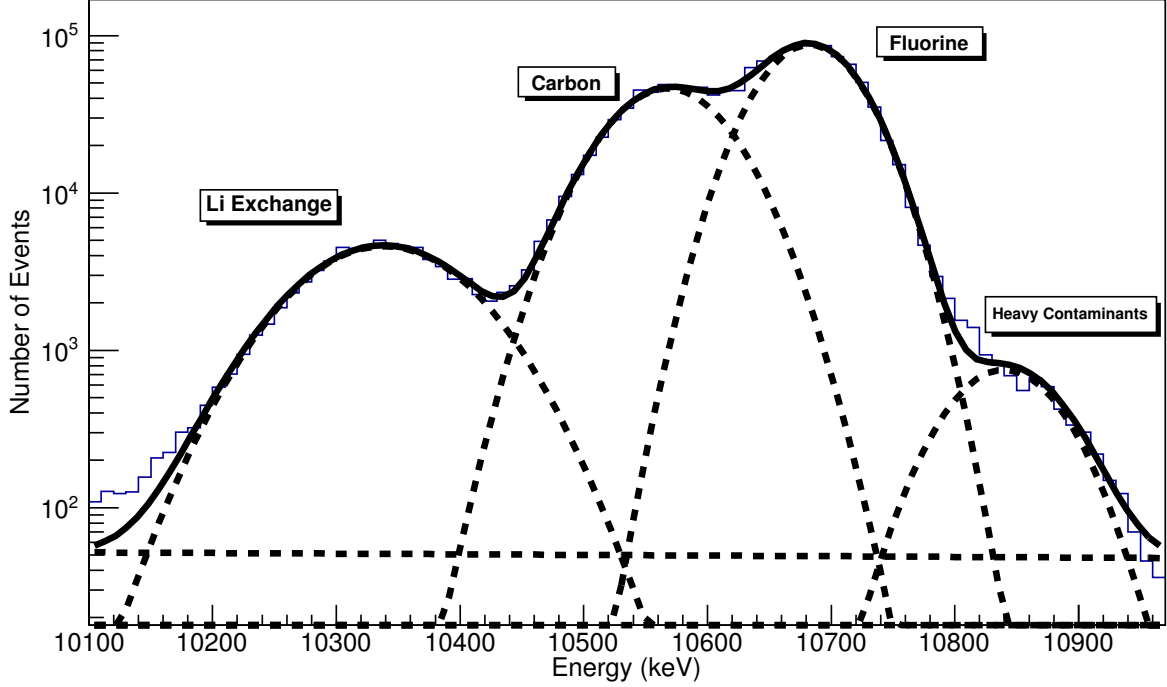
FIG. 3: Data from the S2 detector between 12 and 13 degrees in the laboratory frame. The "Li Exchange" curve represents ^{8}Li and ^{7}Li from the elastic transfer reaction. The two curves labeled "Carbon" and "Fluorine" are ^{8}Li elastically scattered from ^{12}C and ^{19}F respectively. The "Heavy Contaminants" peak is attributed to elastic scattering from trace heavy contaminants.

For the S2 detector the large number of detected events resulted in small statistical errors of $\pm 1.5\%$ or less. The largest sources of error for the S2 are systematics. These errors arise from the extensive measures required to reduce the background and the difficulty in accurately performing multiple peak fits. The estimated systematic errors due to background reduction cuts and fitting are based on their effects on the large peak from the elastic scattering of ^{8}Li from ^{19}F nuclei in the target. Comparing the ratio of the peaks for the ^{19}F scattering before and after implementing background reduction cuts led to an estimated error of $\pm 5\%$ due to the energy and time gates placed on the S2 data. The final source of error for the S2 detector arises from a variation in the determined beam offset position. Varying the offset by 0.10 cm in all directions and comparing the results, a systematic error of $\pm 4.7\%$ from the beam offset is applied to the S2 data.
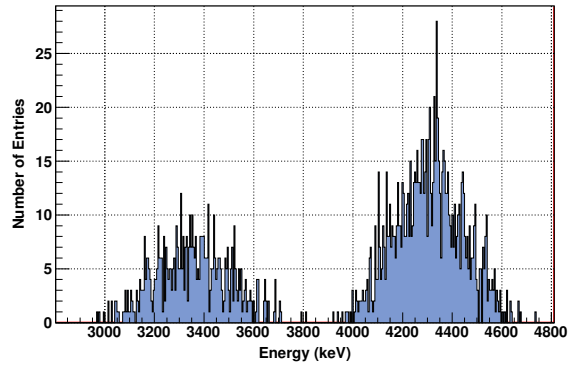
The errors for the data from the LEDA detector arise from similar sources as the errors for the data from the S2 detector; their values however, are notably different. Starting with

7

Energy vs. Scattering Angle
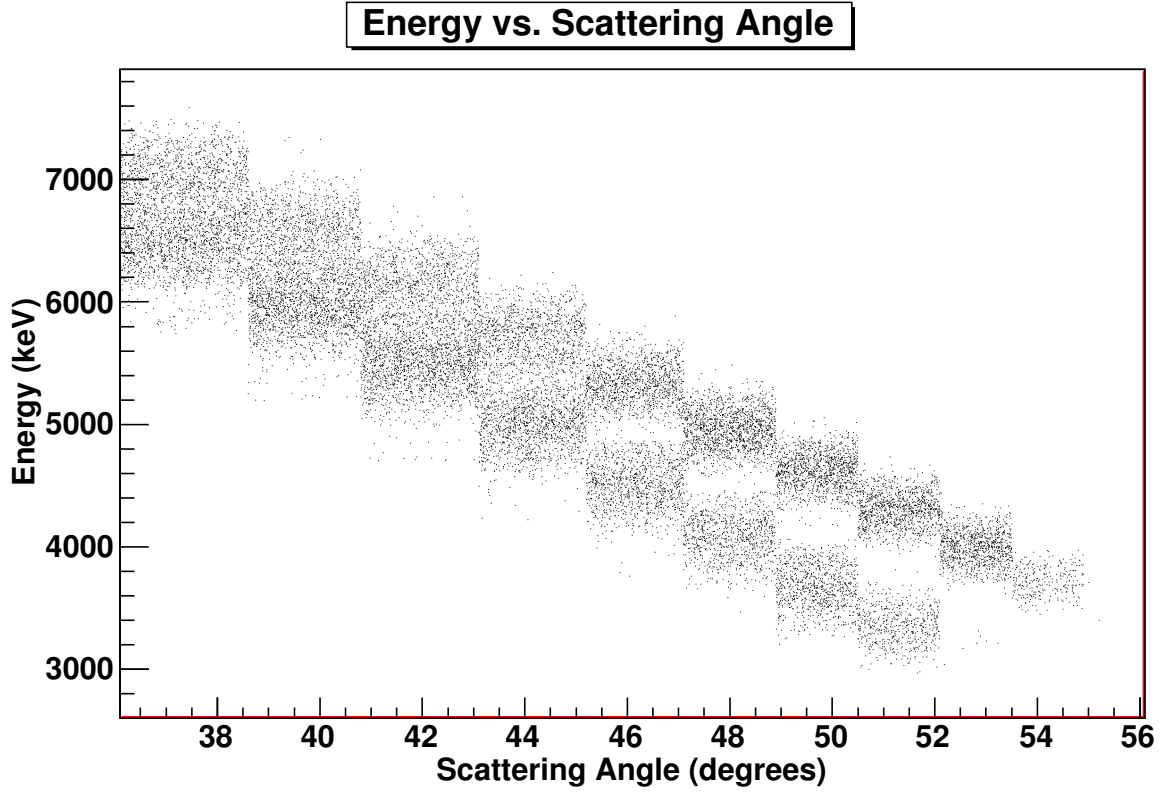
(a)
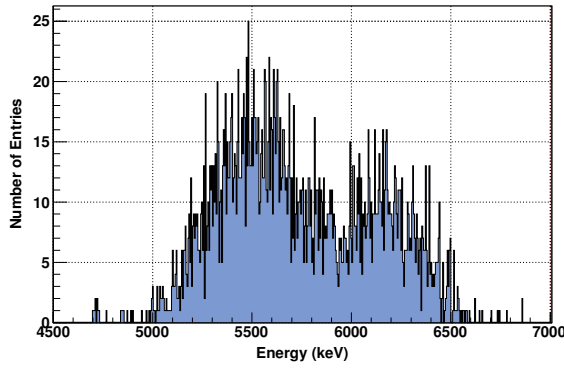
(b)

(c)

FIG. 4: Coincidence events in the LEDA detector are shown in Figure (a). The energy spectra of the $41.0 - 43.1$ degree bin and the $50.5 - 52.0$ degree bin are shown in Figures (b) and (c) respectively. The higher energy locus represents ^{7}Li events and the lower energy locus represents ^{8}Li events.

the much lower statistics for the angular range of the LEDA detector, the statistical errors range from $\pm3\%$ to $\pm6\%$ and are the most significant source of error for the LEDA data. The ability to use a coincidence to separate the ^{8}Li and ^{7}Li from elastic transfer in the LEDA data from the background greatly reduced the size of the systematic errors with respect to the S2 data. Systematic errors due to the placement of the gates on the coincidence events in the LEDA were determined by shifting the position of the gate and comparing the results. Even with unreasonably large shifts applied to the coincidence gate the change in the results was very minimal, translating into a systematic error of only $\pm0.6\%$. The same method of varying the beam offset position as employed for the S2 data results in a systematic error on the LEDA data due to the beam offset of $\pm2.5\%$. This value is lower than the value for the S2 detector due to the rings being larger in the LEDA, and therefore less sensitive to slight offsets from the central position.

Detector	Statistical Error	Systematic Error	Total
S2	0.3-1.5%	6.9%	6.9-7.1%
LEDA	2.8-6.2%	2.6%	3.8-6.7%

TABLE I: Contributions to the point-to-point error for the data from the S2 and LEDA detectors. Total errors are the results of adding the statistical and systematic errors in quadrature.

Total point-to-point errors for the S2 and LEDA detectors after adding the separate sources of systematic error together with the statistical errors in quadrature fall into the range of $\pm4\%$ to $\pm7\%$ and are summarized in Table I. The error associated with the Monte Carlo program used for determining detector geometrical coverage was included with the error values for the beam offset for each detector.

In order to calculate $S_{17}(0)$ from the ^{8}Li ANC the ratio between the mirror system overlap integrals $\left\langle ^8\text{B}(2^+)|^7\text{Be}(\frac{3}{2}^-)\right\rangle$ and $\left\langle ^8\text{Li}(2^+)|^7\text{Li}(\frac{3}{2}^-)\right\rangle$ is required. In Reference [8], the relation between ANCs and charge symmetry breaking nucleon-nucleon (NN) interactions in mirror states was studied. Ratios between mirror ANCs were calculated using two separate effective NN potentials: the Volkov potential V2 [9], and the Minnesota (MN) potential [10]. Averages for the ratios using the two potentials determined in Reference [8] are calculated and shown in Equation 7.

$$\frac{C^2_{p_{1/2}}(^8B)}{C^2_{p_{1/2}}(^8Li)} = 1.22 \pm 0.03$$

$$\frac{C^2_{p_{3/2}}(^8B)}{C^2_{p_{3/2}}(^8Li)} = 1.06 \pm 0.02$$

(7)

Previous measurements of the ^{8}Li neutron ANC from Reference [11], and the ^{8}B proton ANC from Reference [12] were compared with theoretically calculated values in Reference [8]. In both cases the experimentally determined values were much smaller than the calculated values but the ratios were in excellent agreement. Using these ratios along with experimental values for the ANCs, the S factor, $S_{17}(0)$, was calculated; from the V2 potential a value of $S_{17}(0) = 17.8 \pm 1.7$ eV b was obtained, and a value of 18.2 ± 1.8 eV b was obtained using the Minnesota (MN) potential [8]. These calculated values are notably smaller than but consistent with the most recent evaluation, reported by Adelberger *et al.*,

$$S_{17}(0) = 20.8 \pm 0.7(\text{expt}) \pm 1.4(\text{theor}) \text{ eV b}$$

(8)

from Reference [1] which is based on a mean of direct measurements.

For the current study of the ^{7}Li(^{8}Li,^{7}Li)^{8}Li reaction at 11 MeV, no optical potential for the interaction between ^{7}Li and ^{8}Li exists in the literature. Therefore, for our fits using the code FRESCO [13] the initial potential was derived from a study of ^{8}Li elastic scattering data at a laboratory energy between 13 and 20 MeV with targets in the mass range of 1 to 58 amu [14].

In order to reliably fit the large number of free parameters with the limited dataset an initial fit, fixing the spectroscopic amplitudes for the $p_{1/2}$ and $p_{3/2}$ orbitals at theoretical values of 0.0737 and 0.868 respectively from References [15, 16], was performed. The results of this initial fit were used as starting parameters for the optical potential in a new fit where the spectroscopic amplitude for the $p_{3/2}$ orbital was included as a fit parameter. The results from the final fit are summarized in Table II, with the results of the fit displayed in Figure 5.

It was required to add a fitting parameter for the overall normalization of the data as it could not be measured during the experiment due to unreliable readings from the channeltron used for monitoring the beam current. No significant error is expected in the ANC value on account of this problem as the absolute cross section contribution to the ANC error budget

	V (MeV)	r_V (fm)	a_V (fm)	W (MeV)	r_W (fm)	a_W (fm)	norm	$a_{3/2}$
Initial	175	0.64	0.8	16.9	1.09	0.8	9.2×10^{-3}	0.868
Final	173.8	0.500	0.957	5.28	1.514	0.531	9.35×10^{-3}	0.884
Error	2.8	0.008	0.017	0.37	0.021	0.082	0.44×10^{-3}	0.218

TABLE II: Values from FRESCO for the initial and final fits, for the optical potential parameters, normalization, and spectroscopic amplitude of the $p_{3/2}$ orbital, along with the associated errors of the final fit parameters.

is negligible [17], with the shape rather than the magnitude of the differential cross section reflecting the ANC.

The $p_{3/2}$ spectroscopic amplitude is required twice in the FRESCO input file, once for the entrance channel and once for the exit channel. Equations 2 and 3 imply that the differential cross section is proportional to the product of the spectroscopic factors of the entrance and exit channels. Since the spectroscopic amplitudes, $A_{Yal_X j_X}$, are directly related to the spectroscopic factors by the expression

$$S_{Yal_X j_X} = |A_{Yal_X j_X}|^2, \tag{9}$$

the symmetry of the lithium transfer reaction implies that only one of the spectroscopic amplitudes for a given orbital needs to be fitted while the second may remain fixed. The results of the FRESCO fit shown in Table II give the spectroscopic amplitude for the entrance channel $p_{3/2}$ coupling value with the exit channel $p_{3/2}$ coupling value fixed at the initial value of 0.868. From these values the spectroscopic factor S, shown in Equation 2, is calculated to be

$$S_{3/2} = 0.77 \pm 0.19. \tag{10}$$

Due to difficulties during the experiment, two additional runs planned at distinct beam energies were not performed. The theoretical fit to the data is limited to the single dataset from the 11 MeV run discussed so far. This limitation resulted in a larger error than was desired for the final extracted value of the spectroscopic amplitude.

In order to calculate the ANC from the spectroscopic factor, the squared single particle ANC given by the parameter $b_{p_{3/2}}^2(^8\text{Li})$ in Equation 2, is required. In Reference [18], various valence neutron binding potentials were examined for the ^8Li nucleus. The binding potential
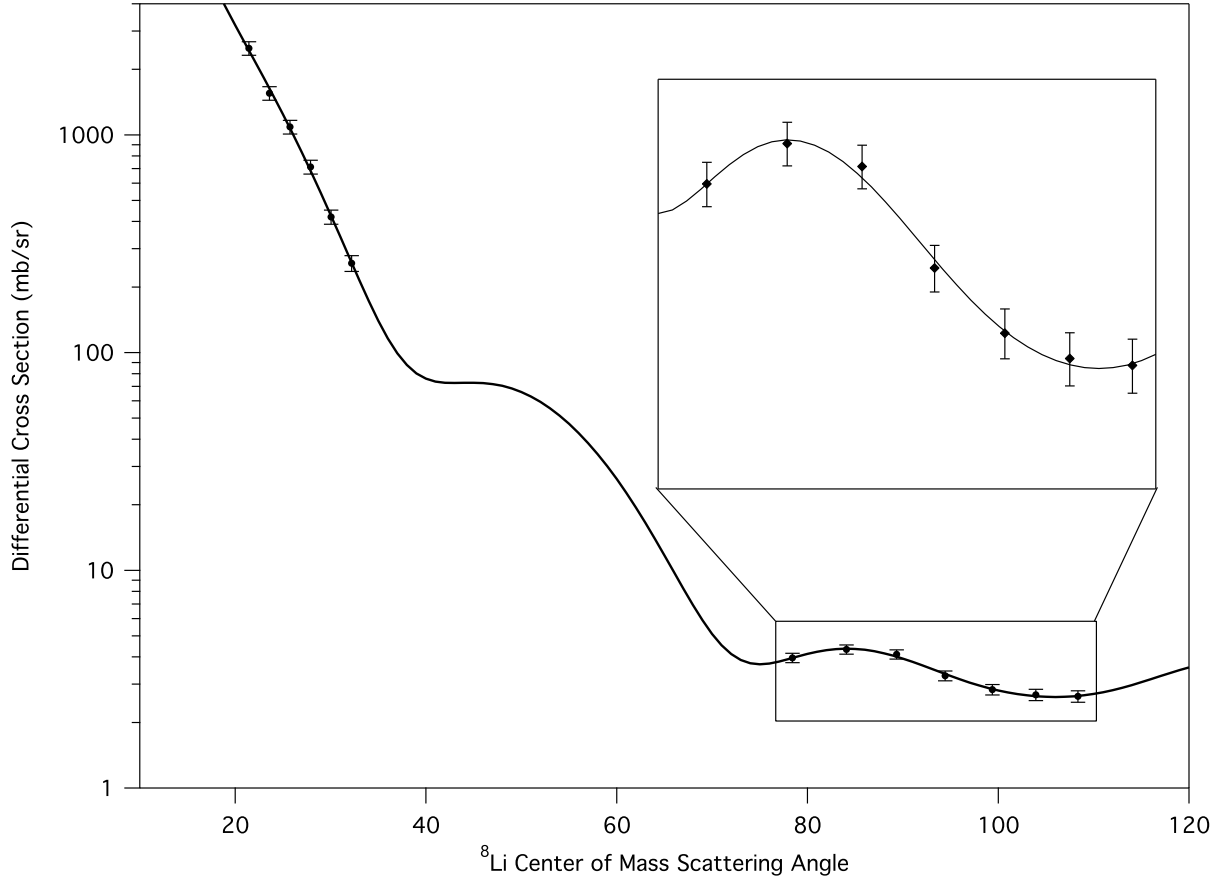
FIG. 5: Angular distribution of the ^{7}Li(^{8}Li, ^{8}Li)^{7}Li reaction at 11 MeV along with the results of the FRESCO calculation corresponding to the final parameters shown in Table II. Experimental data are shown as points with the FRESCO DWBA fit as a solid line.

of Davids and Typel (shown as potential 1 in Table III) produced the best quality of fit of published potentials when the computed bound state wavefunction was compared to the Variational Monte Carlo (VMC) wavefunction of Wiringa [15, 16]. Slight variations of the parameters from the Davids and Typel potential resulted in a new potential which produced an improved quality of fit over the original when compared to the VMC results of Wiringa. The parameters of this new binding potential are shown in Table III as potential 2.

The FRESCO fitting process previously described was performed using potential 2 from Table III. Calculating $C^{2}_{p_{3/2}}$ using the squared single particle ANC value of 0.560 obtained from Reference [18] results in a value of $C^{2}_{3/2}(^{8}\text{Li}) = 0.43 \pm 0.11\,\text{fm}^{-1}$.

A study of ^{13}C(^{7}Li,^{8}Li)^{12}C at 63 MeV [11] resulted in the p$_{3/2}$ and p$_{1/2}$ ^{8}Li ANCs shown

Potential #	V(MeV)	r_V(fm)	a_V(fm)	b^2(fm^{-1})	Ref
1	43.19	2.50	0.65	0.604	[19]
2	43.53	2.50	0.60	0.560	[18]

TABLE III: Binding potentials for the $p_{3/2}$ valence neutron of ^{8}Li with corresponding squared single particle ANC values from Reference [18].

in Table IV. Of particular interest is the ratio

$$\frac{C^2_{p_{1/2}}(^8\text{Li})}{C^2_{p_{3/2}}(^8\text{Li})} = 0.13 \pm 0.02, \tag{11}$$

which was measured for the first time in that study. The error was derived from the uncertainties arising from the angular range used in the fits and uncertainties in the optical potentials.

IV. RESULTS

Lacking angular coverage in this measurement that would allow separate determinations of both the $p_{1/2}$ and $p_{3/2}$ spectroscopic amplitudes, the $p_{1/2}$ ANC must be calculated from the $p_{3/2}$ ANC. The ratio between the two ANC values is taken from Reference [11] and shown in Equation 11. Theoretical calculations using the MN potential have also been shown to agree with this ratio [8]. Using this ratio with the calculated value for $C^2_{p_{3/2}}(^8\text{Li})$ results in $C^2_{p_{1/2}}(^8\text{Li}) = 0.056 \pm 0.016\,\text{fm}^{-1}$. The ANC values for ^{8}Li determined in this study are in agreement with those from Reference [11] and are shown in Table IV.

$C^2_{p_{3/2}}(^8\text{Li})$ (fm^{-1})	$C^2_{p_{1/2}}(^8\text{Li})$ (fm^{-1})	Source
0.384 ± 0.038	0.048 ± 0.006	Ref [11]
0.43 ± 0.11	0.056 ± 0.016	This work

TABLE IV: ^{8}Li ANC values for the $p_{3/2}$ and $p_{1/2}$ orbitals from Reference [11] compared to values from this study.

Using the average of the ratio between the ^{8}Li and ^{8}B ANCs for the V2 and MN potentials from Equation 7, the ^{8}B squared ANCs inferred from this measurement are

$$C^2_{p_{1/2}}(^8\text{B}) = 0.068 \pm 0.020\,\text{fm}^{-1}, \tag{12}$$

13

and

$$C^2_{p_{3/2}}(^8\mathrm{B}) = 0.46 \pm 0.11\,\mathrm{fm}^{-1}. \tag{13}$$

Excellent agreement is observed when comparing these results to previous measurements of Tabacaru *et al.*, $C^2_{p_{1/2}}(^8\mathrm{B}) = 0.052 \pm 0.006$ fm^{-1} and $C^2_{p_{3/2}}(^8\mathrm{B}) = 0.414 \pm 0.043$ fm^{-1} [4]. From the values of the ^{8}B ANCs shown in equations 12 and 13 the astrophysical S factor, $S_{17}(0)$, is calculated from Equation 6,

$$S_{17}(0) = 20.2 \pm 4.4\,\mathrm{eV\,b}. \tag{14}$$

In summary, we have for the first time inferred the ^{8}Li valence neutron ANC using the $^7\mathrm{Li}(^8\mathrm{Li},^7\mathrm{Li})^8\mathrm{Li}$ reaction. Using isospin symmetry with the measured $\mathrm{C}^2_{p_{3/2}}(^8\mathrm{Li})$ the ^{8}B ANCs were calculated and shown to agree with previous results. $S_{17}(0)$, the astrophysical S factor for the radiative capture reaction $^7\mathrm{Be} + \mathrm{p} \rightarrow {}^8\mathrm{B} + \gamma$, was also determined through this measurement and shown to agree with previously published values. Due to the large uncertainty, the present result is consistent with both the radiative capture measurements, and the previous indirect ANC determinations, which imply a smaller value of $S_{17}(0)$. Improvements in the precision of the current result could be achieved with measurements at different ^{8}Li beam energies.

[1] E. G. Adelberger *et al.*, Rev. Mod. Phys. **83**, 195 (2011).

[2] B. W. Filippone, A. J. Elwyn, C. N. Davids, and D. D. Koetke, Phys. Rev. C **28**, 2222 (1983).

[3] A. M. Mukhamedzhanov *et al.*, Phys. Rev. C **56**, 1302 (1997).

[4] G. Tabacaru *et al.*, Phys. Rev. C **73**, 025808 (2006).

[5] H. M. Xu, C. A. Gagliardi, R. E. Tribble, A. M. Mukhamedzhanov, and N. K. Timofeyuk, Phys. Rev. Lett. **73**, 2027 (1994).

[6] T. Davinson *et al.*, Nucl. Instrum. Methods Phys. Res. A **454**, 350 (2000).

[7] J. F. Ziegler, M. Ziegler, and J. Biersack, Nucl. Instrum. Methods Phys. Res. B **268**, 1818 (2010).

[8] N. K. Timofeyuk and P. Descouvemont, Phys. Rev. C **71**, 064305 (2005).

[9] A. Volkov, Nucl. Phys. **74**, 33 (1965).

[10] D. Thompson, M. Lemere, and Y. Tang, Nucl. Phys. A **286**, 53 (1977).

[11] L. Trache *et al.*, Phys. Rev. C **67**, 062801 (2003).

[12] A. Azhari *et al.*, Phys. Rev. C **63**, 055803 (2001).

[13] I. J. Thompson, Comp. Phys. Rep. **7**, 167 (1988).

[14] F. D. Becchetti *et al.*, Phys. Rev. C **48**, 308 (1993).

[15] R. B. Wiringa, "Two-cluster distribution functions," `http://www.phy.anl.gov/theory/research/overlap/` (2011).

[16] I. Brida, S. C. Pieper, and R. B. Wiringa, Phys. Rev. C **84**, 024319 (2011).

[17] S. Burzynski *et al.*, Nucl. Phys. A **399**, 230 (1983).

[18] S. Wright, *ANC for the valence neutron in* ^{8}Li *from a study of* ^{8}Li(^{7}Li,^{8}Li)^{7}Li *a mirrored approach to* $S_{17}(0)$, Master's thesis, University of Surrey, UK (2006).

[19] B. Davids and S. Typel, Phys. Rev. C **68**, 045802 (2003).